BioSystems xxx (xxxx) 104889

Contents lists available at ScienceDirect

BioSystems

journal homepage: www.elsevier.com/locate/biosystems

Modeling the interaction between donor-derived regulatory T cells and effector T cells early after allogeneic hematopoietic stem cell transplantation

Nobuaki Nishiyama [a, b, *], Peter Ruoff [c], Juan Carlos Jimenez [d], Fumikazu Miwakeichi [e], Yoshiaki Nishiyama [a, 1], Tsuyoshi Yata [b]

[a] Division of Mathematical and Physical Sciences, Graduate School of Natural Science and Technology, Kanazawa University, Ishikawa, Japan
[b] Emerging Media Initiative, Kanazawa University, Ishikawa, Japan
[c] Department of Chemistry, Bioscience, and Environmental Engineering, University of Stavanger, Stavanger, Norway
[d] Department of Interdisciplinary Mathematics, Institute of Cybernetics Mathematics and Physics, Havana, Cuba
[e] Department of Statistical Modeling, Institute of Statistical Mathematics, Tokyo, Japan

ARTICLE INFO

Handling Editor: Dr. A.U. Igamberdiev

Keywords:
Regulatory T cells
Computational model
Parameter estimation
Perfect adaptation
Allogeneic hematopoietic stem cell transplantation

ABSTRACT

While allogeneic hematopoietic stem cell transplantation (allo-HSCT) is a potential curative therapy against hematological malignancies, modulation of donor T cell alloreactivity is required to enhance the graft-versus-leukemia (GVL) effect and control graft-versus-host-disease (GVHD) after allo-HSCT. Donor-derived regulatory $CD4^+CD25^+Foxp3^+$ T cells (Tregs) play a central role in establishing of immune tolerance after allo-HSCT. They could be a key target to be modulated for increasing the GVL effect and control of GVHD. We constructed an ordinary differential equation model incorporating bidirectional interactions between Tregs and effector $CD4^+$ T cells (Teffs) as a mechanism for control of Treg cell concentration. The goal is to elucidate how the interaction between Tregs and Teffs is modulated in order to get insights into fine tuning of alloreactivity after allo-HSCT. The model was calibrated with respect to published Treg and Teff recovery data after allo-HSCT. The calibrated model exhibits perfect or near-perfect adaptation to stepwise perturbations between Treg and Teff interactions, as seen in Treg cell populations when patients with relapsed malignancy were treated with anti-CTLA-4 (cytotoxic T lymphocyte-associated antigen 4). In addition, the model predicts observed shifts of Tregs and Teffs concentrations after co-stimulatory receptor IL-2R or TNFR2 blockade with allo-HSCT. The present results suggest simultaneous blockades of co-stimulatory and co-inhibitory receptors as a potential treatment for enhancing the GVL effect after allo-HSCT without developing GVHD.

1. Introduction

Allogeneic hematopoietic stem cell transplantation (allo-HSCT) is a potentially curative therapy for hematological malignancies, due to graft-versus-leukemia (GVL) effect mediated by mature donor T cells (Copelan, 2006; Parmar and Ritchie, 2014). In response to host and/or donor antigen-presenting cells (APCs), allogeneic donor T cells undergo activation and differentiate into effector cell types leading to the elimination of the residual malignant cells, but have also the potential to cause healthy tissue damage. They are crucial for the development of graft-versus-host disease (GVHD), which is the leading cause of morbidity and mortality after allo-HSCT (Copelan, 2006; Parmar and Ritchie, 2014).

Immunosuppressive function of regulatory $CD4^+CD25^+Foxp3^+$ T cells (Tregs) is essential for maintaining self-tolerance in secondary lymphoid organs and inflammation resolution in peripheral tissues (Sakaguchi et al., 2008; Benoist and Mathis, 2012). There is increasing evidence that donor-derived Tregs also play a central role in the establishment of immune tolerance after allo-HSCT (Taylor et al., 2001; Karim et al., 2002; Miura et al., 2004; Zorn et al., 2005).

Interleukin-2 (IL-2) is the essential cytokine for proliferation and suppressive function of Tregs (Malek and Bayer, 2004; Nelson, 2004;

* Corresponding author. Division of Mathematical and Physical Sciences, Graduate School of Natural Science and Technology, Kanazawa University, Ishikawa, Japan.
E-mail address: nnishiya@staff.kanazawa-u.ac.jp (N. Nishiyama).
[1] Present address: Clinical Research Support Center Kyushu, Fukuoka, Japan.

https://doi.org/10.1016/j.biosystems.2023.104889
Received 7 October 2022; Received in revised form 12 March 2023; Accepted 29 March 2023
0303-2647/

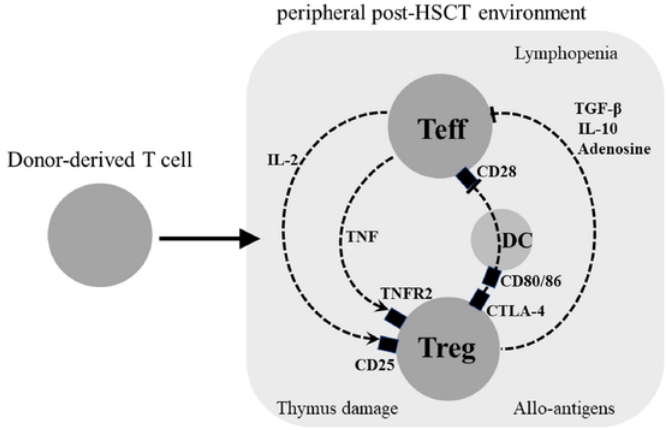

Fig. 1. Interaction between donor-derived regulatory T cells and effector Tcells after allogeneic hematopoietic stem cell transplantation (allo-HSCT). After allo-HSCT, donor-derived T cells in the periphery are exposed to endogenous factors including lymphopenia, allo-antigen and thymus damage. Activations and inhibitions of Treg and Teff proliferation via cytokines as well as co-stimulatory and co-inhibitory receptors are described by dashed lines with arrowheads and blunt bars, respectively.

Toomer and Malek, 2017). IL-2 is produced mainly by donor derived $CD4^+$ T cells in the setting of allo-HSCT (Via and Finkelman, 1993). Deficient recovery of Tregs in posttransplant lymphopenic environment including IL-2 caused $CD4^+$ T cells deficiency, is associated with the occurrence of GVHD (Matsuoka et al., 2010). Consistent with this, low-dose IL-2 administration enables to selectively stimulate Tregs with the high affinity IL-2 receptor and improves GVHD (Matsuoka et al., 2013). Using anti-CD25(IL-2 receptor) microbeads to deplete Tregs from donor lymphocyte infusions (DLI) enhances GVL, which is associated with an improved survival in patients that relapsed after allo-HSCT. On the other hand, the treatment of Tregs depletion leads also to significantly accelerated GVHD (Nikiforow et al., 2016). In summary, Tregs could be a key target to be modulated for increasing the GVL effect or controlling GVHD. The mechanisms underlying the control of Tregs concentration need to be clarified for fine-tuning or modulation of immune responses early after allo-HSCT.

Accumulating evidence suggests that activation-inhibition configuration between Tregs and effector $CD4^+(CD45RO^+CD27^-$ and $CD45RO^-CD27^-$) T cells (Teffs) is one of the central mechanisms underlying Treg homeostasis (Roychoudhuri et al., 2015; Liu et al., 2015). $CD4^+CD45RO^+CD27^-$ T cells constitute the effector subset, and $CD4^+CD45RO^-CD27^-$ T cells constitute the terminal effector subset. While IL-2 is essential for the generation and suppressive function of Tregs, Tregs do not produce IL-2. IL-2 is produced predominantly by Teffs responding to self- or nonself-antigen. Tregs with a higher expression of CD25(IL-2Rα) preferentially consume IL-2, thereby limiting the amount of available IL-2 for Teffs (Setoguchi et al., 2005; Amado et al., 2013). In addition to Tregs expansion and their functional activation by IL-2, multiple mechanisms of Teff-mediated enhancement of Treg expansion and Treg-mediated suppression of Teffs activation shape the activator-inhibitor system. Tregs with enriched IL-2 have significantly higher expression of co-inhibitory receptor cytotoxic T lymphocyte–associated antigen (CTLA-4). CTLA-4 competes with co-stimulatory receptor CD28 on Teffs in binding to common ligands CD80/CD86 on dendritic cells (DC), or strip them from DC, thereby reducing the co-stimulatory signals that Teffs receive (Sansom, 2000; Winga et al., 2021). Tregs also secrete immunosuppressive cytokines like interleukin-10 (IL-10) and transform growth factor-β(TGF-β), which can suppress Teff proliferation. In addition to IL-2, Tumor necrosis factor (TNF) is produced by activated Teffs and enhances Treg expansion via its co-stimulatory TNF receptor 2 (TNFR2) (Baeyens et al., 2015). Cell contact-dependent inhibition of Teffs by Tregs has also been reported to be through cAMP transfer via gap junctions (Klein and Bopp, 2016).

In this work, we hypothesize that the core regulatory network underlying the control of Treg concentration early after allo-HSCT is the feedback loops between Tregs and Teffs, as shown in Fig. 1.

Based on this hypothesis, we construct an ordinary differential equation model to describe how varying bidirectional interactions between Tregs and Teffs by co-stimulatory and/or co-inhibitory receptors blockades influence the dynamic features of Tregs and Teffs. Several modeling studies (Groß et al., 2011, 2011d; de Mendizábal et al., 2011) of immune response regulation have focused on the bidirectional interaction between Tregs and Teffs, especially on IL-2 mediating interaction between Tregs and Teffs (Feinerman et al., 2010; Höfer et al., 2012; Almeida et al., 2012; Khailaie et al., 2020). Our model is based on experimentally proposed crosstalk (Sansom, 2000; Winga et al., 2021; Baeyens et al., 2015; Köhler et al., 2021; Perry et al., 1101) between Tregs and Teffs via co-stimulatory and co-inhibitory receptors and is parameterized based on clinical data (Matthews et al., 2009). In our model, the bidirectional interactions between Tregs and Teffs are based on Hill functions. While Vélez de Mendizábal et al. proposed a model with Hill functions for the cross-regulatory interactions between the Teff and Treg populations (de Mendizábal et al., 2011), a fit to clinical data and parameter estimation was not performed.

To validate our model in the clinical setting, we estimate model parameters by fitting the model to published time series data of Treg and Teff recoveries after allogeneic hematopoietic stem cell transplantation (allo-HSCT) (Matthews et al., 2009). Thymus-dependent generation of donor T cells early after allo-HSCT is commonly compromised in adults because of thymic damage resulting from high-dose chemotherapy and irradiation administered as part of the myeloablative regimen. Early T lymphocyte recovery after allo-HSCT depends on spontaneous peripheral expansion of mature T cells that are present in the stem cell graft and could be approximated to be thymus-independent process.

Our validated model shows how the balance between Tregs and Teffs is modulated by co-stimulatory and co-inhibitory receptor blockades, which suggest therapeutic approaches to improve alloreactivity and the GVL effect after allo-HSCT.

1.1. Computational methods

The differential equations were numerically solved with the Matlab function ode23 using the explicit Runge-Kutta 3(2) pair of Bogacki and Shampine formulas (BogackiPShampine, 1989) with automatic step-size (Ver. 9.9.0; The Mathworks, Inc.). Nullclines and steady states were analyzed with the MATLAB function fsolve. Parameter estimation was performed via the Innovation Method (Ozaki and Bozdogan, 1994) by using the algorithms developed in (Jimenez, 2020; Jimenez et al., 2021) with global optimization (Gonzalez-Arenas et al., 2021). This inference method is robust, not confined to local optimum parameters, and is effective even for a small number of noisy discrete observations with missing data. In order to see the influence of certain parameters, step-wise changes in parameter values were employed.

2. Results

The regulation of Teffs by Tregs shows a close relationship to a de-repression negative feedback loop with autocatalysis (Drengstig et al., 2012a; Drobac et al., 2021). Fig. 2 shows the robust perfect adaptation of this motif, where A is the homeostatic regulated species and E is the regulator. A and E correspond to Teff and Treg, respectively.

The behavior of perturbation-compensatory homeostasis suggests a potential mechanism of lymphocyte homeostasis. In the present study, the feedback loop in Fig. 2 was extended to the model sketched in Fig. 3, which describes the homeostasis of Teffs in the periphery early after allo-HSCT.

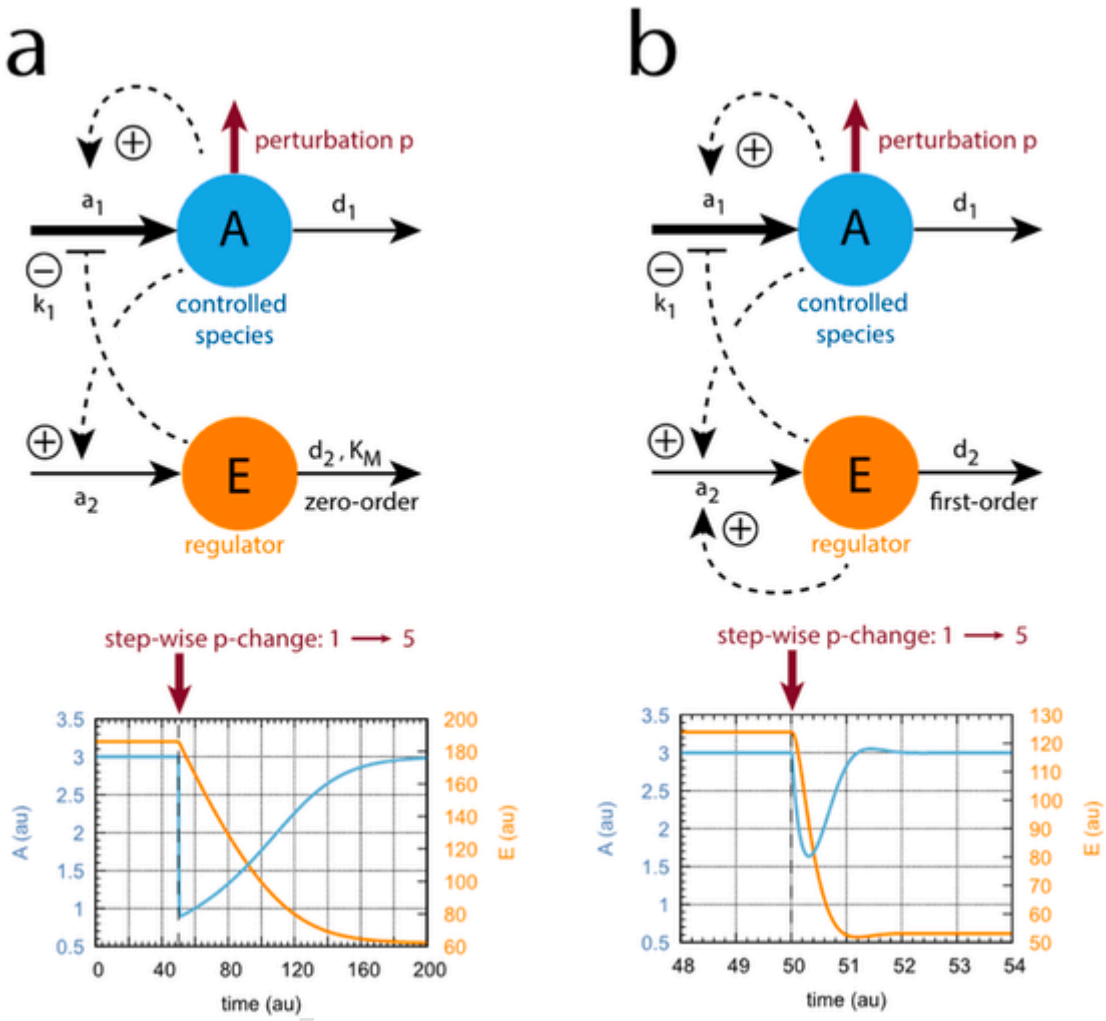

Fig. 2. Basic negative feedback structure in T-cell regulation and a comparison between non-autocatalytic and autocatalytic regulators. In this example, species A is under integral control, which allows for robust perfect adaptation in A when step-perturbations are applied (Drengstig et al., 2012a; Drobac et al., 2021; Warwick, 1996). Panel a: Robust perfect adaptation in A occurs by integral control due to a zero-order removal of regulator E. Lower graph shows a calculation when p is changed from 1 to 5 at time t = 50 (red arrow). The set-point of A is 3.0. Panel b: The inclusion of autocatalysis in the generation of the regulator E dramatically improves the relaxation time of the controller under otherwise identical conditions (Drengstig et al., 2012b). To keep integral control the removal of E needs to be of first-order with respect to E. See Supporting Material "Autocatalytic versus non-autocatalytic regulation" for details.

Early T lymphocyte recovery during 6–12 months after allo-HSCT is dependent on the spontaneous peripheral expansion of mature T cells that are present in the stem cell graft, but T cell recovery can be delayed for more than 2 years (Dekker et al., 2020). Therefore, we assume that early recovery of Teffs and Tregs could be approximated to be a thymus-independent process.

The model sketched in Fig. 3 is translated into the following set of differential equations:

$$\frac{d\left[T_{eff}\right]}{dt} = a_E\left(\frac{k_{REi}^2}{k_{REi}^2+\left[T_{reg}\right]^2}\right)\left(\frac{k_{EEi}}{k_{EEi}+\left[T_{eff}\right]}\right)\left[T_{eff}\right] - d_E\left[T_{eff}\right], \quad (1)$$

$$\frac{d\left[T_{reg}\right]}{dt} = a_R\left(\frac{\left[T_{eff}\right]^2}{k_{ERa}^2+\left[T_{eff}\right]^2}\right)\left(\frac{k_{RRi}}{k_{RRi}+\left[T_{reg}\right]}\right)\left[T_{reg}\right] - d_R\left[T_{reg}\right]. \quad (2)$$

$[T_{eff}]$ and $[T_{reg}]$ are the respective concentrations of Teff cells ($CD4^+(CD45RO^+CD27^-$ and $CD45RO^-CD27^-$) T cells) and Treg cells ($CD4^+CD25^+Foxp3^+$ T cells).

The spontaneous peripheral proliferation of mature T cells relies on the support of homeostatic cytokines as well as allogeneic antigens encountered in the host. In the model, both spontaneous peripheral proliferations of donor-derived Teff and Treg cells are considered to be autocatalytic with rate constants a_E and a_R. The contributions of homeostatic cytokines and allogeneic antigen stimulation are lumped into the rate equations. The thymic-dependent generation of T cells is not considered. Self-inhibitions of the spontaneous proliferation of both Teffs and Tregs are incorporated into the model, where the expansion of programmed cell death ligand 1 (PD-L1) expressing T cells is suppressed via ligation of programmed cell death protein 1 (PD-1) on neighboring

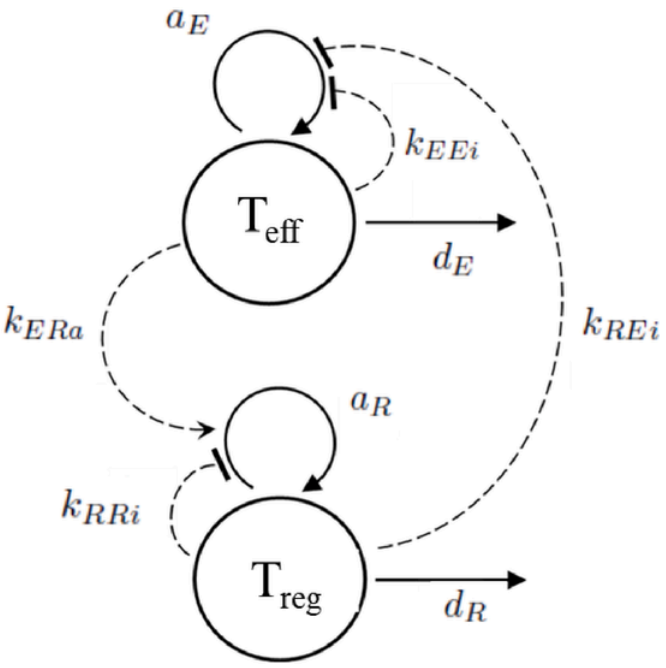

Fig. 3. Sketch of the model for the bidirectional regulation between Teffs and Tregs. a_E and a_R are the spontaneous proliferation rates of Teffs and Tregs, respectively. d_E and d_R are the clearance rates of Teffs and Tregs, respectively. The k_{REi}, k_{EEi}, k_{ERa}, k_{RRi} are activation and inhibition constants. Activations and inhibitions are described by dashed lines with respectively arrowheads and blunt bars. The k subscripts 'a' and 'i' indicate activation and inhibition, respectively.

T cells (Diskin et al., 2020; Perry et al., 1101). The self-inhibitions of Teff and Treg proliferation are modeled as Hill functions with the inhibition constants k_{EEi} and k_{RRi}, respectively.

The model's bidirectional regulation of Teff and Treg cells is based on the following observations. Teff cell-dependent Treg cell proliferation can be activated through IL-2 and/or TNF (Baeyens et al., 2015; Cohen and Wood, 2018a). Paracrine IL-2 and TNF produced in an antigen-dependent fashion by Teffs are essential resources for the survival and proliferation of Tregs. These two cytokines can directly activate the proliferation of Tregs that express a high level of the high-affinity IL-2 receptor CD25 (IL-2Rα) and TNFR2 (Baeyens et al., 2015; Cohen and Wood, 2018a). The concentrations of IL-2 and TNF can, in good approximation, be regarded as proportional to the Teff concentration and therefore do not explicitly appear in the model. In addition, cross-linking of PD-1 and PD-1 ligand 1 (PD-L1) on Teffs induces the conversion from Teffs to highly suppressive Tregs (Fanelli et al., 2021). This Teff-dependent activation of the Treg population is lumped together as a Hill function with the activation constant k_{ERa} and a Hill coefficient of $n = 2$. Tregs inhibit the proliferation, survival and function of Teffs through multiple mechanisms. CTLA-4 expressed highly by Tregs enables them to inhibit the costimulatory capacity of dendritic cells (DCs) by sequestration of CD80 and CD86 on the surface of DCs, thereby leading to the inhibition of Teff proliferation (Sansom, 2000; Winga et al., 2021). Adenosine and cytokines IL-10 and TGF-β produced by Tregs inhibit Teffs proliferation directly or via inhibition of DC presentation of antigens. Because of the effect of cAMP via gap junctions mentioned in the Introduction, in the model, these Tregs-dependent inhibitions of Teffs proliferation are assumed to be proportional to Treg concentration and are lumped together to be modeled as a Hill function with the inhibition constant k_{REi} and the Hill coefficient $n = 2$. The clearance of Teffs and Tregs is assumed to be proportional to each concentration with the rates d_E and d_R, respectively. Our preliminary considerations about the dependency of the system's dynamics on the value of the Hill coefficients showed that the model with $n = 1$ never exhibited perfect adaptations. However, the model with $n = 2$ exhibited the behavior of perfect adaptation combined with randomly selected values of the other parameters. We think a higher value of the Hill coefficient is a strong assumption. As a result, in the present study, we assume the value of the Hill coefficients is 2 in the present study.

The model described above was fitted to the clinical of the previous work by Matthews et al. (2009). They assessed the relationship of the kinetics of T cell reconstitution with the incidence of Graft-versus-host-disease (GvHD) in patients ($n = 25$) undergoing allo-HSCT for myeloid malignancies. The transplant preparative regimen included the administration intravenously of fludarabine, busulphan, and alemtuzumab leading to in vivo lymphocyte depletion. Peripheral blood samples were collected immediately prior to conditioning for the transplant and at days 30, 60, 90, 180, 270, and 360 after transplantation.

Samples of peripheral blood were also collected from 11 healthy age-matched volunteers. A significant Treg deficit in the group that developed acute GVHD was observed at day 30 and the median Treg/Teff ratio was 0.24% compared to 0.83% for patients without GVHD. Later, the Treg population gradually increased in all patients, and the median Treg/Teff ratio at day 180 in patients ($n = 4$) who developed chronic GVHD is 33% compared to 10% for patients without GVHD. Three of the four patients with chronic GVHD and higher Treg/Teff ratio subsequently experienced leukemia relapse. Fig. 4a shows the recoveries of $CD4^+$ cells and $CD4^+CD25^+Foxp3^+$cells (Tregs) in the periphery after allo-HSCT. Each plot denotes the median cell number of 25 patients by 12 months, which was still below the median values of 1183 (cells/μL) ($CD4^+$ cells) and 57 (cells/μL) (Tregs) for 11 age-matched healthy volunteers because of thymus damage following cytoreductive regimens and dominant expansion of donor derived T cells in the periphery.

On the other hand, the recovery kinetics of Treg and of effector $CD4^+$($CD45RO^+CD27^-$and $CD45RO^-CD27^-$) T (Teff) cell numbers for one of the four patients with chronic GvHD and subsequent leukemia relapse is shown in Fig. 4b. We used the Innovation Method with global optimization (Jimenez, 2020; Jimenez et al., 2021; Gonzalez-Arenas et al., 2021) for estimating parameters in the ordinary differential equations (1) and (2). The solid lines in Fig. 4a and b show responses of the model with parameter values estimated by fitting to median numbers of T cells at time points in 25 patients and by fitting to T cell numbers in one patient with chronic GvHD having later relapse, respectively.

For the parameter estimation, the cell number of $CD4^+$ cells in Fig. 4a was roughly approximated to be equal to that of effector $CD4^+$($CD45RO^+CD27^-$ and $CD45RO^-CD27^-$) T cells (Teffs). For completeness, Table 1 presents the estimated values of the model parameters for the data of Fig. 4a and b. Specifications on the model fitting to the data are provided in the Appendix.

Fig. 5ashows the response to steps up in the parameter k_{ERa} while the parameter k_{REi} is kept constant. Simulation is started from the steady state corresponding to a state of potential relapse risk, which is obtained with the estimated parameter values of Table 1 corresponding to the data of Fig. 4b.

Perfect and near-perfect adaptation of Teff cell numbers to a stepwise increase in k_{ERa} is observed, while the steady state of Treg cell numbers depends on the values of k_{ERa} (Fig. 5b). Fig. 5c and d shows that when k_{ERa} is fixed to its initial steady state ($k_{ERa} = 8.2760$), perfect and near-perfect adaptation in Treg cell numbers occur when k_{REi} values increase stepwise while Teff cell numbers depend on k_{REi}. Finally, when keeping k_{REi} at its value ($k_{REi} = 16.8515$), the cell number of Tregs is decreased, and Teffs are increased by stepwise increases of k_{ERa} (Fig. 5e).

We are interested in the model's therapeutic implications for increasing the GVL effect and controlling of GVHD. While GVHD occurrence after allo-HSCT has been described for specific T cell numbers, there is growing evidence that the ratio of Treg cell numbers to $CD4^+$ T cell numbers is also associated with GVHD occurrence. To assess the

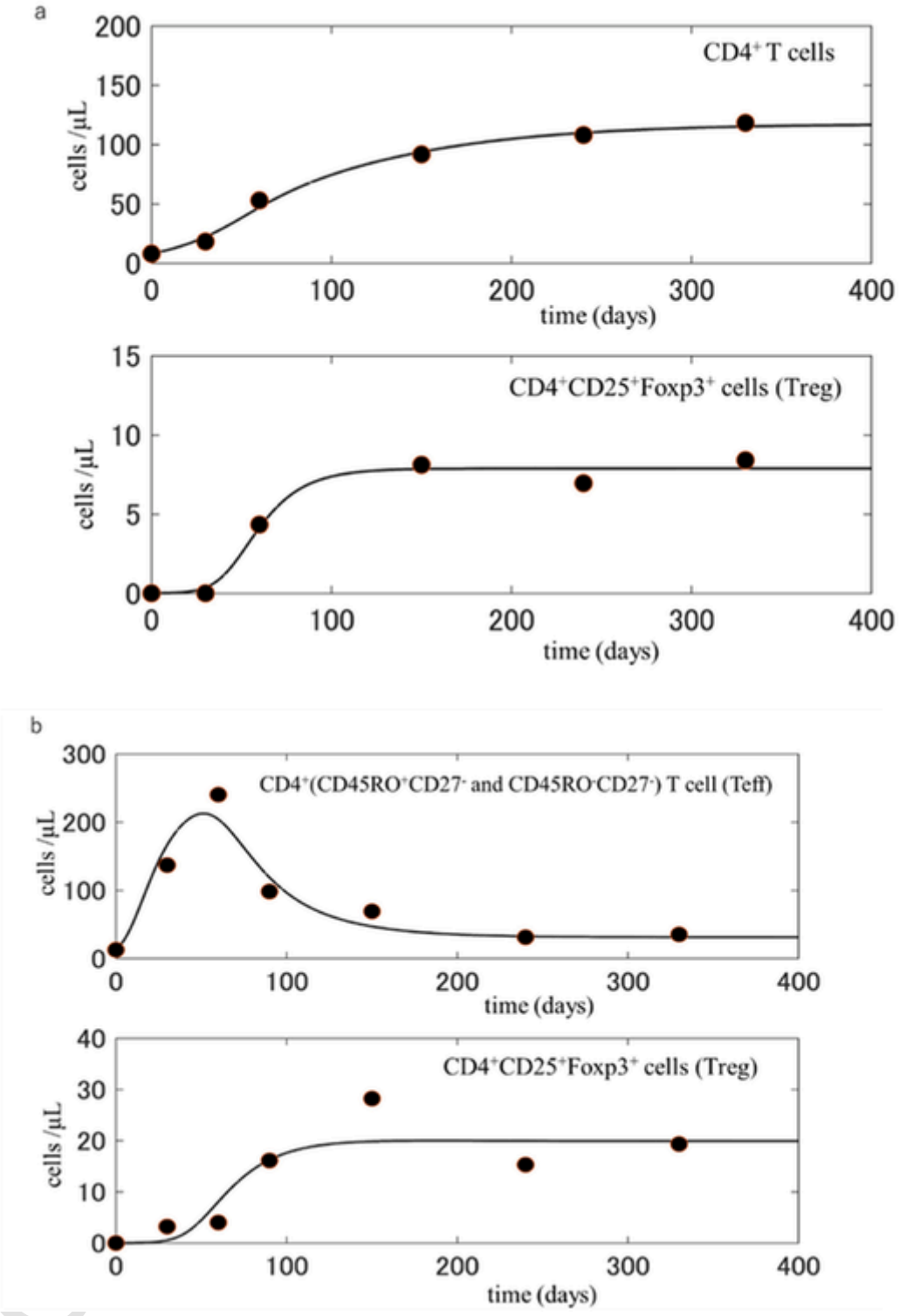

Fig. 4. Time courses (closed circles) of cell numbers of T cells extracted from lymphocyte recovery after allogeneic hematopoietic stem cell transplantation reported by Matthews et al. (Matthews et al., 2009). Solid lines show the cell numbers of Teffs and Tregs obtained by the numerical integration of equations (1) and (2) with the parameter values of Table 1 estimated by the Innovation Method. (a) Closed circles show median cell numbers of $CD4^+$ cells (upper) and $CD4^+CD25^+Foxp3^+$ cells (Tregs) (lower) of 25 patients. Calculated time courses of cell numbers of Teffs (upper) and Tregs (lower) were obtained with initial cell numbers of $[Teff]_0 = 8.16(cells/\mu L)$, $[Treg]_0 = 0.01(cells/\mu L)$ and parameter values of Table 1. (b) Closed circles show the recovery dynamics of cell numbers of Teff (upper) and Treg (lower) for one of the four patients with chronic GvHD and later leukemia relapse. Calculated time courses of cell numbers of Teffs (upper) and Tregs (lower) were obtained with initial cell numbers of $[Teff]_0 = 12.90(cells/\mu L)$, $[Treg]_0 = 0.01(cells/\mu L)$ and parameter values of Table 1.

Table 1
Estimated value of the model parameters from the data of Fig. 4a and b with 90% of confidential interval. To avoid over-parametrization in the model estimation, the data of the variable Treg of the model were shifted in 0.1 days in time (see Appendix).

Parameter	Parameter values for the data of Fig. 4a	Parameter values for the data of Fig. 4b
a_E (/day)	0.0679 ± 0.0034	0.2963 ± 0.0003
d_E (/day)	0.0270 ± 0.0001	0.0979 ± 0.0001
k_{REi} (cells/μL)	15.2877 ± 4.3072	16.8515 ± 0.5953
k_{EEi} (cells/μL)	119.4473 ± 8.7209	118.9507 ± 0.1655
a_R (/day)	0.2355 ± 0.0010	0.2049 ± 0.0002
d_R (/day)	0.0943 ± 0.0002	0.0663 ± 0.0001
k_{ERa} (cells/μL)	3.4657 ± 1.4605	8.2760 ± 0.1479
k_{RRi} (cells/μL)	5.2828 ± 0.0557	9.6828 ± 0.0108

Table 2
List of abbreviations.

Abreviation	Definition
allo-HSCT	allogeneic hematopoietic stem cell transplantation
GVL	graft-versus-leukemia
GVHD	control graft-versus-host-disease
CTLA-4	cytotoxic T lymphocyte–associated antigen 4
IL-2	interleukin-2
IL-2R	interleukin-2 receptor
TNF	tumor necrosis factor
TNFR2	tumor necrosis factor receptor 2
APC	antigen-presenting cell
DLI	donor lymphocyte infusions
DC	dendritic cell
IL-10	interleukin-10
TGF-β	transforming growth factor-β
PD-L1	programmed cell death ligand 1
PD-1	programmed cell death protein 1
PBMC	peripheral blood mononuclear cell

safety and efficacy of checkpoint inhibitors used in conjunction with allo-HSCT, studies reported that a Treg/Teff ratio of less than 9% is associated with increased incidence and severity of GVHD (Merryman et al., 2017; Pang et al., 2015; Fujioka et al., 2013). GVL effect correlated positively with an increasing risk of GVHD occurrence (Baron et al., 2020). Therefore, we assume that a Treg/Teff ratio of 9% is a critical threshold between GVHD and GVL effects. Fig. 6 shows Treg/Teff steady state concentration as a function of the parameters k_{REi} and k_{ERa}. Fig. 6 suggests that a larger value of k_{REi} or k_{ERa} corresponding to respective receptor blockade could force to shift the system from the state with potential relapse risk (red dots) to the state with lower relapse risk (blue dots).

Fig. 7a shows the time-courses of Teff and Treg cell numbers, in which the system responds to a step of k_{ERa} followed by a return to the original steady state with a time delay. When Treg is generated by a non-autocatalytic mechanism, the approach to the steady states is significantly slower (see Supporting Material "Autocatalytic versus non-autocatalytic regulation).

Fig. 7b shows the corresponding phase plane trajectories from the time courses in Fig. 7a. While the Teff nullcline of the system is kept fixed, the Treg nullcline changes with increasing values of k_{ERa} and a corresponding shift in the system's steady state. It may be noted that the location of the steady state is not changed for k_{ERa} values larger than 348.6(cells/μL). The system spends considerable time near this steady state before returning to the original steady state, because the trajectory from this steady state moves along the slow Teff nullcline. The resulting time delay for returning to the original steady state is associated with the steady state of higher Teff cell numbers. The delay lasts for a significant time, even after resetting to the original value of k_{ERa}. This suggests a durable prevention of relapse after the withdrawal of a co-stimulatory receptor blockade.

3. Discussion

A fundamental assumption in our description of Treg cell number is that the activation-inhibition configuration shaped by Treg - Teff interactions plays a central role in regulating the Treg/Teff ratio. Activation - inhibition mechanisms between Tregs and Teffs were the subject of a number of mathematical models of antigen-stimulated T cells. The feedback loops between Tregs and Teffs via IL-2 have been extensively modeled, wherein IL-2 produced predominantly by Teffs acts as an autocrine growth factor and simultaneously promotes Treg expansion. In turn, IL-2 consumption by expanded Tregs leads to decreasing Teff cell numbers (Groß et al., 2011, 2011d; de Mendizábal et al., 2011; Feinerman et al., 2010; Höfer et al., 2012; Almeida et al., 2012; Khailaie et al., 2020). Vélez de Mendizábal et al. proposed a model, which describes how cross-regulation between Tregs and Teffs after antigen stimulation contributes to the relapsing – remitting dynamics of an autoimmune disease (de Mendizábal et al., 2011). Their model considers the interactions between Tregs and Teffs with Hill functions. They found that changes in a given parameter move the steady state to higher numbers of Teff, while Treg cell numbers remain practically the same, similar to the perfect and near-perfect adaptations of Treg cell numbers shown in Fig. 5c. On the other hand, we focused on the spontaneous proliferation of T cells in the periphery after allo-HSCT without naïve T cell output from the thymus. This allowed us to estimate model parameters by using time series data, and to make predictions on both, the allo-HSCT and the treatments including co-stimulatory and co-inhibitory receptors blockades.

Other models were used to describe $CD4^+$ T cell reconstitution after the allo-HSCT in pediatric patients with a range of hematological disorders (Hoare et al., 2017), and in patients with autologous HSCT and hematological malignancies (Baliu-Pique et al., 2021). From the data of 288 patients after the allo-HSCT, basal values of proliferation rates and clearance rates were respectively estimated to be 0.207 (/day) and 0.477 (/day), with the estimated value of 0.216 (cells/day) for the inflow rate from thymus (Hoare et al., 2017). The clearance rate is an order of magnitude larger than our estimates in Table 1. The larger value of clearance rate might be originated from the inclusion of the $CD4^+$ cell inflow into the model of (Hoare et al., 2017), which is valid for rapid thymic reconstitution after pediatric allo-HCST. On the other hand, our estimated clearance rates are similar to those of the memory $CD4^+$ T cells estimated from data of autologous HCST patients fitting to the model without a thymic output (range; 0.0108–0.0549 (/day)). On the other hand, the proliferation rates of the memory $CD4^+$ T cells in the autologous HSCT patients range from 0.0109 (/day) to 0.0541 (/day) (Baliu-Pique et al., 2021), which are smaller than the rates estimated in the present study. This discrepancy may be due to the slower recovery of the T cells after autologous HSCT relative to the allo-HSCT.

The co-inhibitory receptor CTLA-4 is constitutively expressed on Treg cells and limits the co-stimulatory activity of DCs by removing CD80/CD86 on their cell surface, leading to Teff cell inhibition. Zhou et al. performed a clinical trial of CTLA-4 blockade in patients with relapse of hematological malignancy after allo-HSCT (Zhou et al., 2011). Almost all relapsed patients before the CTLA-4 blockade (by a CTLA-4 monoclonal antibody ipilimumab) had a significantly higher percentage of Treg cells than the normal controls, despite their $CD4^+$ lymphopenia associated with allo-HSCT. Furthermore, the authors of (Zhou et al., 2011) found that Teff cell numbers in peripheral blood significantly increased after ipilimumab infusion, while no significant change in the Treg cell numbers was observed. This finding is consistent with

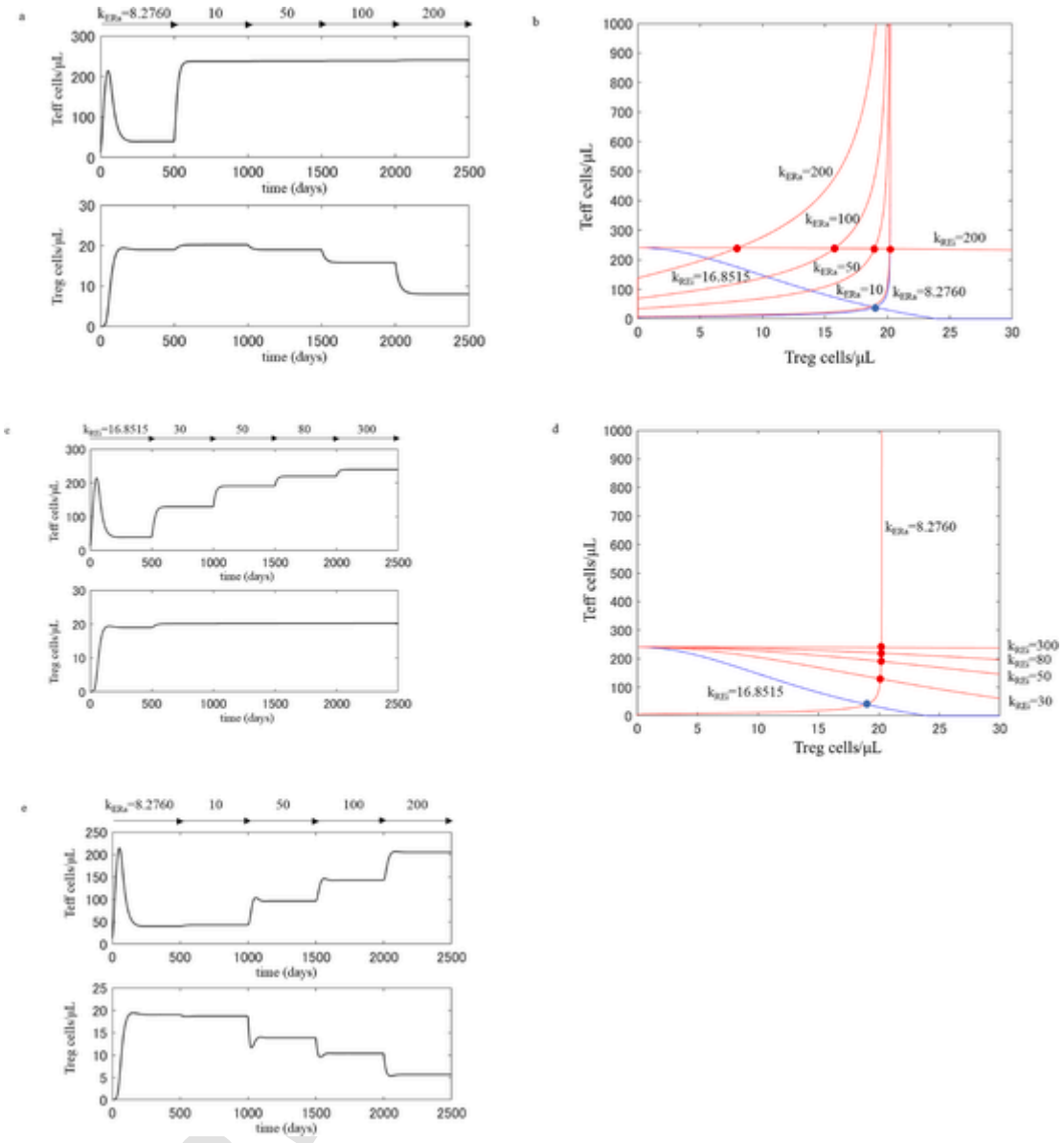

Fig. 5. The model's response to step perturbations in the parameters k_{REi} and k_{ERa}. (a) Initial steady state is obtained with k_{REi} = 16.8515(cells/μL) and k_{ERa} = 8.2760(cells/μL) (Fig. 4b). With k_{REi} = 200(cells/μL), the system exhibits perfect and near-perfect adaptation in Teff cell numbers when k_{ERa} is stepwise increased. (b) The blue closed circle denotes the initial steady state as the intersection of two blue nullclines with k_{REi} = 16.8515(cells/μL) and k_{ERa} = 8.2760(cells/μL). With stepwise increased values of k_{ERa}, the steady state denoted by the red closed circle moves along the nullcline with k_{REi} = 200(cells/μL). (c) Initial steady state as in panel a. With the constant value of k_{ERa} = 8.2760(cells/μL), the system exhibits perfect and near-perfect adaptation in Treg cell numbers when k_{REi} is stepwise increased. (d) The blue dot denotes the initial steady state where the two nullclines with k_{REi} = 16.8515(cells/μL) and k_{ERa} = 8.2760(cells/μL) intersect. With stepwise increased values of k_{REi}, the steady state denoted by the red dot moves along the nullcline with k_{ERa} = 8.2760(cells/μL). (e) When keeping k_{REi} at its initial steady state (k_{REi} = 16.8515(cells/μL)), the cell number of Tregs is decreased and that of Teffs is increased when k_{ERa} increases stepwise. Initial cell numbers are $[Teff]_0$ = 12.90(cells/μL), $[Treg]_0$ = 0.01(cells/μL), and the values of the remaining parameters a_E, a_R, d_E, d_R, k_{EEi}, and k_{RRi} are the estimated for the data of Fig. 4b as reported in Table 1.

the perfect or near-perfect adaptation predicted by our model in Fig. 5c, where the CTLA-4 blockade has no influence on the Treg cell numbers. Additionally, Zhou et al. found that no Treg depletion with enhanced Teff cell numbers by the CTLA-4 blockade is associated with productively low rates of the GVHD.

On the other hand, as shown in Fig. 5e, our model predicts that blockade of Treg cell activation by Teffs leads to Treg depletion with elevated Teff cell numbers. Treg activation by Teffs is part of a negative feedback mechanism to limit inflammatory and autoimmune responses. In this mechanism, IL-2 is produced predominantly by the activated Teffs and is consumed by Tregs with the high affinity IL-2 receptor, which leads to Treg expansion with enhanced suppressive functions. IL-2 receptor alpha chain (CD25) and the tumor necrosis factor receptor-type 2 (TNFR2) (which induce higher Treg expression rates relative to activated Teffs) have been considered as potential targets for Treg cell depletion in order to enhance the GVL effect in patients who relapsed after allo-HSCT. Locke et al. reported the effect of the CD25 blockade with Daclizumab (a monoclonal antibody) on Treg reconstitution after allo-HSCT in patients with hematologic malignancies or severe aplastic anemia (Locke et al., 2017). Daclizumab was administered by 5 weekly intravenous infusions followed by a long-term analysis of peripheral blood T cells. Daclizumab decreased the percentage of Tregs in $CD4^+$ cells at days 11–35 compared with placebo, and this decrease was maintained up to days 101. The percentage of central memory cells in

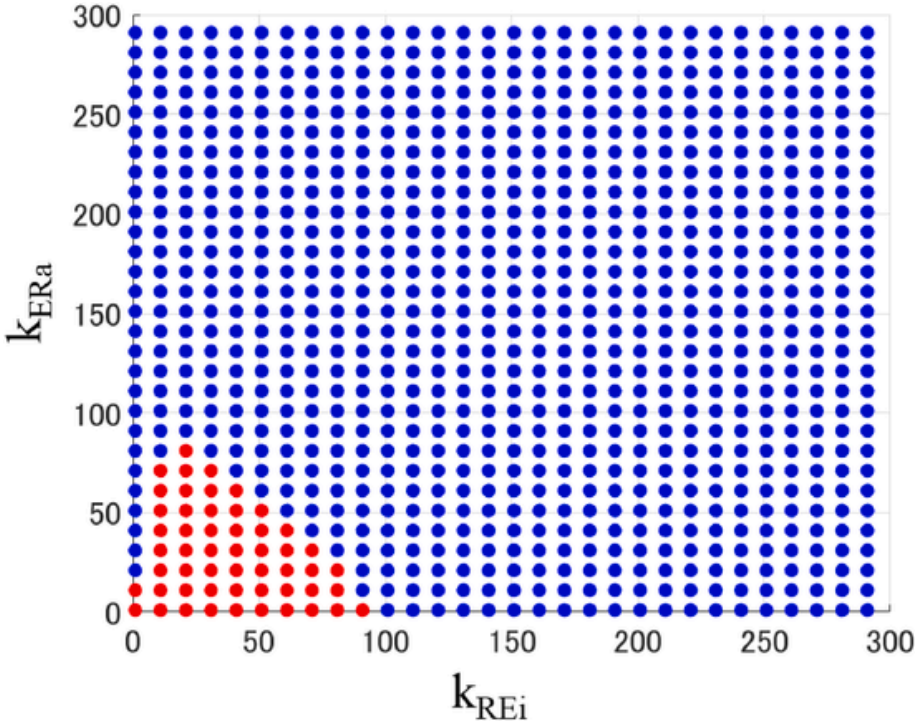

Fig. 6. Treg/Teff steady state ratios as a function of the parameters k_{REi} and k_{ERa}. The red dots show Treg/Teff ratios larger than 9%, which suggests potential relapse risk. Blue dots show Treg/Teff ratios of 9% or less indicating a potential occurrence of GVHD. Each steady state was arrived from initial cell numbers of $[Teff]_0 = 12.90$(cells/μL), $[Treg]_0 = 0.01$(cells/μL) with parameter values a_E, a_R, d_E, d_R, k_{EEi}, and k_{RRi} of Table 1 corresponding to the data of Fig. 4b. The integration time was of 1000 days.

$CD4^+$ cells at days 11–35 and days 81–101 revealed an increasing trend compared with placebo, although these differences were statistically insignificant. In line with Treg cell depletion by the CD25 blockade, Moatti et al. reported donor-derived Treg cell depletion with TNFR2 blockade in experimental conditions that mimic patients with hematological malignancy relapse after HSCT (Moatti et al., 2022). TNF is a cytokine abundantly produced during the cytokine storm following allo-HSCT and has been demonstrated to boost proliferation and the suppressive functions of Tregs, as Treg express higher levels of TNFR2 compared to other T cells (Cohen and Wood, 2018b). In their study, human peripheral blood mononuclear cells (PBMCs) from healthy volunteers were pre-treated with an anti-human TNFR2 antibody or a control immunoglobulin and injected intravenously into immunodeficient NSG. The analysis of spleens on day six showed that the percentage of $FOXP3^+$Tregs in the $CD4^+$ cells was lower than that in control mice. At the same time, the percentage of $FOXP3^-$ Teffs in the $CD4^+$ was higher in the treated mice than in the control (Moatti et al., 2022). Such Treg depletion and Teff expansion by the CD25 or TNFR2 blockade is consistent with our prediction from blocking Treg cell activation by Teffs.

In this work, we focused on how the balance between Tregs and Teffs is modulated depending on the model parameters k_{REi} and k_{ERa}, which correspond to the strength of Teff inhibition by Treg and the strength of Treg activation by Teff, respectively. Our model predicts that larger values of k_{ERa} lead to lower Treg/Teff ratios which may be beneficial in enhancing the GVL effect after allo-HSCT, as shown in Fig. 5a and e. Additionally, as it is shown in Fig. 7, we found that the system spends considerable time in the vicinity of the steady state at larger k_{ERa}, before returning to its original steady state, suggesting a prolonged Treg depletion after treatments. As shown in Fig. 5a, larger values of k_{ERa} with increased levels of k_{REi} lead to lower Treg/Teff ratios and perfect adaptation in Teff cell numbers. This is of special interest, giving the possibility for an enhanced GVL effect without developing GVHD in patients who relapsed after allo-HSCT. As larger values of k_{ERa} could be related to the CD25 or TNFR2 blockade and larger values of k_{REi} could be related to the CTLA-4 blockade on Treg cells, the present results suggest that simultaneous blockade of these co-stimulatory and co-inhibitory receptors appears to be a potential treatment for enhancing GVL effect after allo-HSCT without developing GVHD.

The present model assumes that the cell inflows from the thymus are negligible, applying for early after allo-HSCT. In the application for longer post-HSCT, the incorporation of cell inflows of Teffs and Tregs and their autocatalytic activations is in progress.

4. Conclusion

To clarify how the Treg/Teff ratio early after allo-HSCT is changed in dependence on the strength of Teff inhibition by Treg and Treg activation by Teff, we constructed a mathematical model, which includes bidirectional regulation between Tregs and Teffs as a mechanism of Treg homeostasis. The predictions from the model calibrated to T cell recovery after allo-HSCT qualitatively explain the modulation of Tregs and Teffs concentrations after co-stimulatory or co-inhibitory receptor blockade and suggest simultaneous blockade of these receptors as a potential treatment for enhancing GVL effect after allo-HSCT without developing GVHD. Our model, which is yet to be further assessed against clinical observations, may provide insights into fine-tuning of alloreactivity after allo-HSCT. (see Table 2)

Declaration of competing interest

The authors have no conflict of interest directly relevant to the content of this article.

Data availability

Data will be made available on request.

a

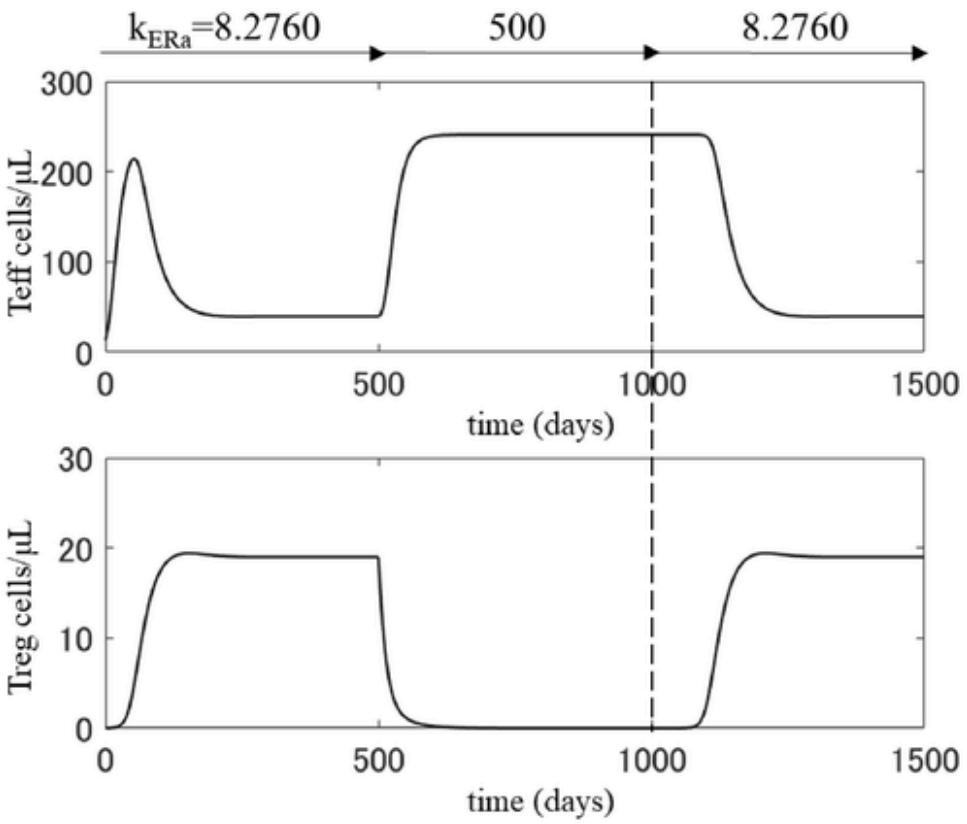
k_{ERa}=8.2760
500
8.2760
Teff cells/μL
300
200
100
0
0
500
1000
1500
time (days)
Treg cells/μL
30
20
10
0
0
500
1000
1500
time (days)

b

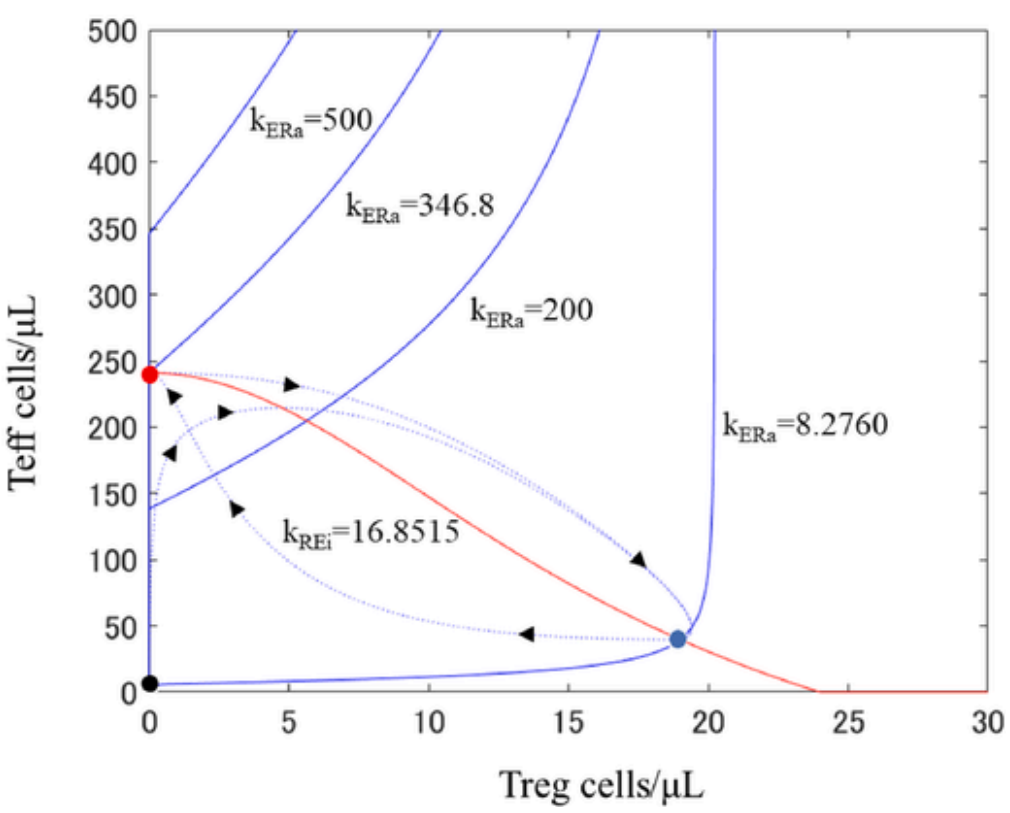
Teff cells/μL
500
450
400
350
300
250
200
150
100
50
0
k_{ERa}=500
k_{ERa}=346.8
k_{ERa}=200
k_{ERa}=8.2760
k_{REi}=16.8515
0
5
10
15
20
25
30
Treg cells/μL

Fig. 7. Time delay accompanying with a return from the steady state of higher cell numbers of Teffs and lower cell numbers of Tregs to the original steady state of lower cell numbers of Teffs. (a) Initial steady state is obtained with values $k_{REi} = 16.8515$(cells/μL) and $k_{ERa} = 8.2760$(cells/μL) estimated for the data of Fig. 4b. With $k_{REi} = 16.8515$(cells/μL) fixed, the system arrives at the steady state of higher Teff cell numbers when a $k_{ERa} = 500$(cells/μL) step is applied at time t = 500 days. When k_{ERa} is returned to its original value of 8.2760(cells/μL) at time t = 1000 days, the system returns to the original steady state with a significant time delay. (b) Phase plane trajectories corresponding to the time course in Fig. 7a are shown. The trajectory from the state of initial cell numbers $[Teff]_0 = 12.90$(cells/μL), $[Treg]_0 = 0.01$(cells/μL) (black dot) moves to the initial steady state indicated by the blue dot. After k_{ERa} is changed to 500(cells/μL), the trajectory moves to the steady state denoted by the red dot and then returns to the original steady state with a time delay. The blue lines show the nullclines of d[Treg]/dt = 0 at different k_{ERa} values. The location of the steady state denoted by the red dot is not changed when k_{ERa} values are larger than 348.6(cells/μL). The values of the parameters a_E, a_R, d_E, d_R, k_{EEi}, and k_{RRi} were set as in Table 1 for the data of Fig. 4b.

Appendix A. Supplementary data

Supplementary data to this article can be found online at https://doi.org/10.1016/j.biosystems.2023.104889.

AppendixSpecifications on the model fitting to the data.

An over-fitted model is a mathematical model that contains more parameters than can be justified by the data. It is known that if the number of parameters of a model is the same as or greater than the number of observations, then the model can perfectly predict the data. That is the case of the proposed 8-parameters model (1)–(2) for the original data of the Fig. 4a (with 6 observations of the variables (Teff, Treg)), and the case of the original data of Fig. 4b (with 7 observations of the same variables). For this reason, for the estimation of the 8 parameters of the model (1)–(2), the original data were modified to be treated as time series with "missing data" in the following way:

Original data corresponding to Fig. 4a

$\{Teff(t_0), Teff(t_1), Teff(t_2), Teff(t_3), Teff(t_4), Teff(t_5)\}$

$\{Treg(t_0), Treg(t_1), Treg(t_2), Treg(t_3), Treg\ (t_4), Treg\ (t_5)\}$,

being $\{t_0,t_1,t_2,t_3,t_4,t_5,\}$ the 6 time instants where the original data were collected.

Modified data for the parameter estimation

$\{Teff(T_0), Teff(T_1), -, Teff(T_3), -, Teff(T_5), -, Teff(T_7), -, Teff(T_9)\}$

$\{Treg(T_0), -, Treg(T_2), -, Treg(T_4), -, Treg(T_6), -, Treg\ (T_8), -, Treg\ (T_{10})\}$

with.

$T = \{t_0,t_1,t_1+s,t_2,t_2+s,t_3,t_3+s,t_4,t_4+s,t_5,t_5+s\}$,

where s = 0.1 (day) is a small time shift and the symbol "-" means missing value. At this point, we recall that each pair of available values of (Teff, Treg) are the average of those collected from 25 patients at one specific day, probably at different hours, which implies that the time accuracy of such measurements is of at least 24 h. In addition, since the 6 available values of the variables (Teff, Treg) are given in the period of almost a year with at least a month of difference among each observation, the time shift of 0.1 day is negligible in the considered scale of time. Moreover, we conducted numerical experiments where we estimated the 8-parameters model using the modified-type of data generated with different values of time shift (in the rage of a few hours). In no case were there significant differences in the values of the estimated parameters. Taking all of this into account, we set the time shift s = 0.1 day to carry out the parameter estimation from the modified set of data as specified above. In this way, the 8 parameters of the model were estimated from the values of the variables Teff and Treg at 11 instants of time. Similarly, for the second set of original data, the 8 parameters of the model were estimated from the values of the variables Teff and Treg at 13 instants of time.

The value of this strategy to avoids over-parameterization is illustrated with a model selection analysis that includes six simplified models. The six simplified models were respectively obtained by fixing the parameters $a_E = 1$, $a_R = 1$, $a_E = a_R = 1$, $d_E = 0$, $d_R = 0$, and $k_{ERa} = 0$ in the proposed 8-parameters model (1)–(2). By using the same inference procedure specified above, we estimate the six or seven parameters of these simplified models from the two sets of data. Table 3 presents the log likelihood (LogLK) and the Akaike Information Criteria (AIC) of each fitted model to the data of Fig. 4a and b. According with the results of that table, the 8-parameters model is the one with the minimum AIC value for both sets of data, that is, the 8-parameters model presents the best trade-off between goodness of fit and simplicity for these data. Moreover, the second better-fitted model, the 7-parameters model (1)–(2) with $k_{ERa} = 0$, is only $\exp((2047.2 - 2074.8)/2) = 10^{-6}$ times as probable as the 8-parameters model to minimize the information loss for the data of Fig. 4a, and it has much lower probability for the data of Fig. 4b. In summary, among the considered models, the proposed 8-parameters model (1)–(2) is the best choice to describe the two given sets of data.

Table 3
Log likelihood (LogLK) and the Akaike Information Criteria (AIC) of the seven models fitted to the data of Fig. 4a and b.

Data of Fig. 4a	Model (1)–(2) with $a_E = 1$	Model (1)–(2) with $a_R = 1$	Model (1)–(2) with $a_E = a_R = 1$	Model (1)–(2) with $d_E = 0$	Model (1)–(2) with $d_R = 0$	Model (1)–(2) with $k_{ERa} = 0$	Model (1)–(2)
LogLK	-3.30×10^{7}	-9.16×10^{5}	-5.70×10^{6}	-2.54×10^{6}	-2.00×10^{7}	−1030.4	−1015.6
AIC	6.61×10^{7}	1.83×10^{6}	1.14×10^{7}	5.08×10^{6}	4.01×10^{7}	2074.8	2047.2
Data of Fig. 4b							
LogLK	-3.93×10^{6}	-1.29×10^{6}	-1.51×10^{6}	-4.40×10^{7}	-1.13×10^{6}	−135024	−70901.2
AIC	7.87×10^{6}	2.59×10^{6}	3.02×10^{6}	8.81×10^{7}	2.26×10^{6}	270062	141818.4

In addition, figures Figs. 8 and Fig 9 present the profile likelihood keeping fixed 7 of the 8 parameters of the model (1)–(2) fitted to the data of Fig. 4a and b. In both cases, the likelihood function reaches a maximum value at the estimated parameter value.

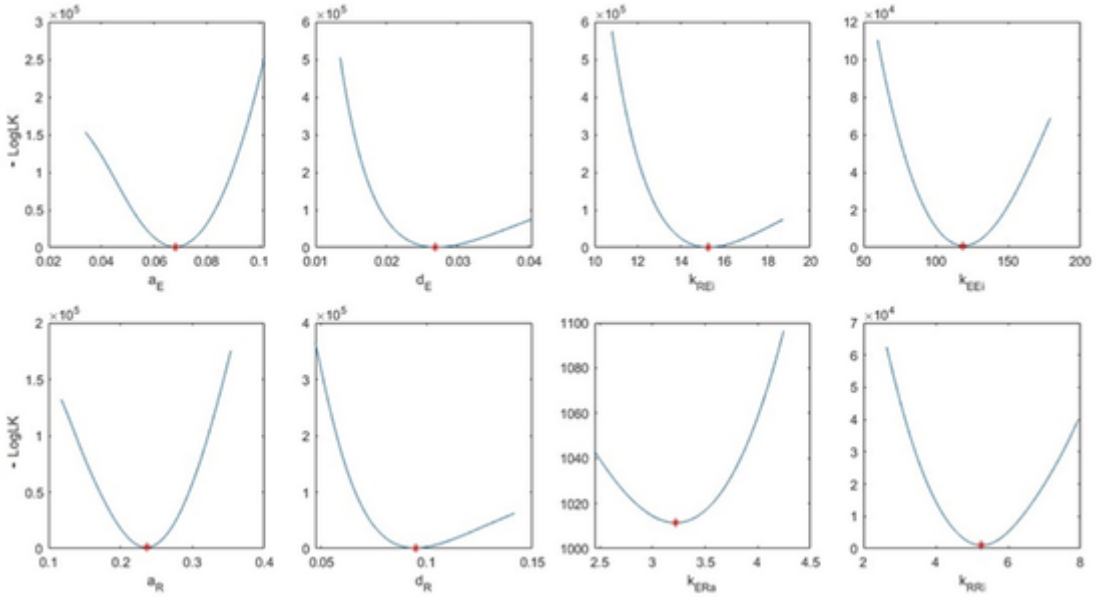

Fig. 8. Profile likelihood keeping fixed 7 of the 8 parameters of the model (1)–(2) fitted to the data of Fig. 4a. In each subplot, "*" highlights the pair (p,-LogLK (p)), where p is the estimated value of the corresponding parameter specified in Table 1 and LogLK(p) = −1015.6 is the log likelihood for the 8 values of p.

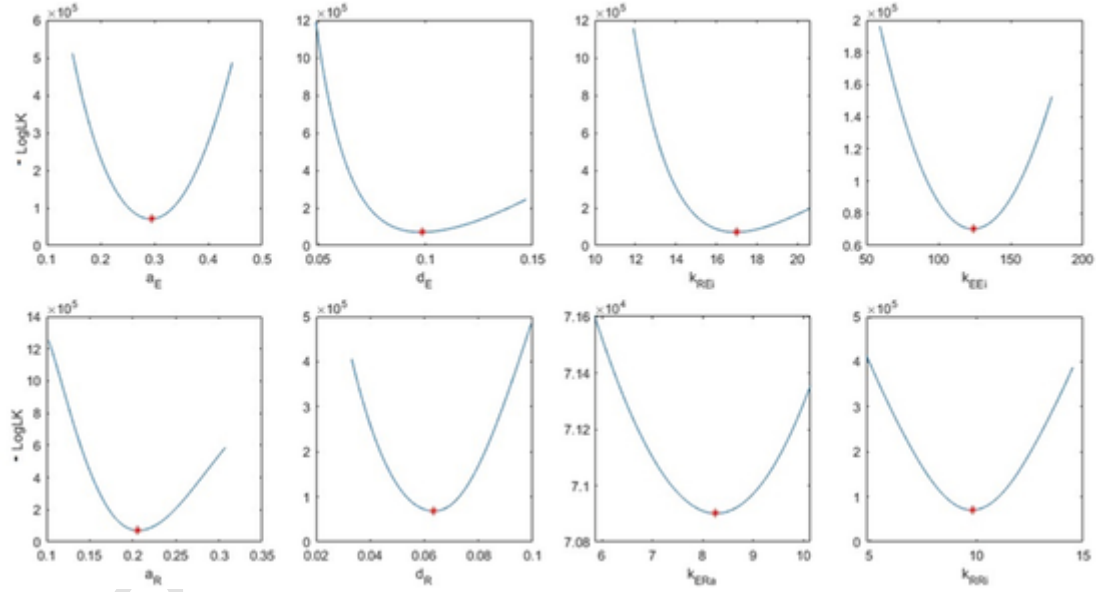

Fig. 9. Profile likelihood keeping fixed 7 of the 8 parameters of the model (1)–(2) fitted to the data of Fig. 4b. In each subplot, "*" highlights the pair (p,-LogLK (p)), where p is the estimated value of the corresponding parameter specified in Table 1 and LogLK(p) = −70901.2 is the log likelihood for the 8 values of p.

References

Almeida, A.R.M., Amado, I.F., Reynolds, J., Berges, J., Lythe, G., Molina-París, C., Freitas, A.A., 2012. Quorum-sensing in CD4$^+$ T cell homeostasis: a hypothesis and a model. Front. Immunol. 3, 125.

Amado, I.F., Berges, J., Luther, R.J., Mailhé, M., Garcia, S., Bandeira, A., Weaver, C., Liston, A., Freitas, A.A., 2013. IL-2 coordinates IL-2–producing and regulatory T cell interplay. J. Exp. Med. 210, 2707–2720.

Baeyens, A., Saadoun, D., Billiard, F., Rouers, A., Gregoire, S., Zaragoza, B., Grinberg-Bleyer, Y., Marodon, G., Piaggio, E., Salomon, B.L., 2015. Effector T cells boost regulatory T cell expansion by IL-2, TNF, OX40, and plasmacytoid dendritic cells depending on the immune context. J. Immunol. 194, 999–1010.

Baliu-Pique, M., van Hoeven, V., Drylewicz, J., van der Wagen, L.E., Janssen, A., Otto, S.A., van Zelm, M.C., de Boer, R.J., Kuball, J., Borghans, J.A.M., Tesselaar, K., 2021. Cell-density independent increased lymphocyte production and loss rates post-autologous HSCT. Elife 10, e59775.

Baron, F., Labopin, M., Savani, B.N., Beohou, E., Niederwieser, D., Eder, M.E., Potter, V., Kroger, N., Beelen, D., Socie, G., Itala-Remes, M., Bornhauser, M., Mohty, M., Nagler, A., 2020. Graft-versus-host disease and graft-versus-leukaemia effects in secondary acute myeloid leukaemia: a retrospective, multicentre registry analysis from the Acute Leukaemia Working Party of the EBMT. Br. J. Haematol. 188, 428–437.

Benoist, C., Mathis, D., 2012. Treg cells, life history, and diversity. Cold Spring Harbor Perspect. Biol. 4, a007021.

Bogacki, P., P, Shampine, L.F., 1989. A 3(2) pair of Runge - kutta formulas. Appl. Math. Lett. 2, 321–325.

Cohen, J.L., Wood, K.J., 2018a. TNFR2: the new Treg switch? Oncoimmunol 7, e1373236.

Cohen, J.L., Wood, K.J., 2018b. TNFR2: the new Treg switch? Oncoimmunol 7, e1373236.

Copelan, E.A., 2006. Hematopoietic stem-cell transplantatio. N. Engl. J. Med. 354, 1813–1826.

de Mendizábal, N.V., Carneiro, J., Solé, R.V., Goñi, J., Bragard, J., Martinez-Forero, I., Martinez-Pasamar, S., Sepulcre, J., Torrealdea, J., Bagnato, F., Garcia-Ojalvo, J., Villoslada, P., 2011. Modeling the effector-regulatory T cell cross-regulation reveals the intrinsic character of relapses in Multiple Sclerosis. BMC Syst. Biol. 5, 114.

Dekker, L., de Koning, C., Lindemans, C., Nierkens, S., 2020. Reconstitution of T Cell subsets following allogeneic hematopoietic cell transplantation. Cancers 12, 1974.

Diskin, B., Adam, S., Cassini, M.F., Sanchez, G., Liria, M., Aykut, B., Buttar, C., Li, E., Sundberg, B., Salas, R.D., Chen, R., Wang, J., Kim, M., Farooq, M.S., Nguy, S., Fedele,

C., Tang, K.H., Chen, T., Wang, W., Hundeyin, M., Rossi, J.A.K., Kurz, E., Haq, U., M.I, Karlen, J., Kruger, E., Sekendiz, Z., Wu, D., Shadaloey, S.A.A., Baptiste, G., Werba, G., Selvaraj, S., Loomis, C., Wong, K., Leinwand, J., Miller, G., 2020. PD-L1 engagement on T cells promotes self-tolerance and suppression of neighboring macrophages and effector T cells in cancer. Nat. Immunol. 21, 441–452.

Drengstig, T., Jolma, I.W., Ni, X.Y., Thorsen, K., Xu, X.M., Ruoff, P., 2012a. A basic set of homeostatic controller motifs. Biophys. J. 103, 2000–2010.

Drengstig, T., Ni, X.Y., Thorsen, K., Jolma, I.W., Ruoff, P., 2012b. Robust adaptation and homeostasis by autocatalysis. J. Phys. Chem. B 116, 5355–5363.

Drobac, G., Waheed, Q., Heidari, B., Ruoff, P., 2021. An amplified derepression controller with multisite inhibition and positive feedback. PLoS One 16 (3), e0241654.

Fanelli, G., Romano, M., Nova-Lamperti, E., Sunderland, M.W., Nerviani, A., Scottà, C., Bombardieri, M., Quezada, S.A., Sacks, S.H., Noelle, R.J., Pitzalis, C., Lechler, R.I., Lombardi, G., Becker, P.D., 2021. PD-L1 signaling on human memory CD4+Tcells induces a regulatory phenotype. PLoS Biol. 19, e3001199.

Feinerman, O., Jentsch, G., Tkach, K.E., Coward, J.W., Hathorn, M.M., Sneddon, M.W., Emonet, T., Smith, K.A., Altan-Bonnet, G., 2010. Single-cell quantification of IL-2 response by effector and regulatory T cells reveals critical plasticity in immune response. Mol. Syst. Biol. 6, 437.

Fujioka, T., Tamaki, H., Ikegame, K., Yoshihara, S., Taniguchi, K., Kaida, K., Kato, R., Inoue, T., Nakata, J., Ishii, S., Soma, T., Okada, M., Ogawa, H., 2013. Frequency of CD4(+)FOXP3(+) regulatory T-cells at early stages after HLA-mismatched allogeneic hematopoietic SCT predicts the incidence of acute GVHD. Bone Marrow Transplant. 48, 859–864.

Gonzalez-Arenas, Z., Jimenez, J.C., Lozada-Chang, L., Santana, R., 2021. Estimation of distribution algorithms for the computation of innovation estimators of diffusion processes. Math. Comput. Simulat. 187, 449–467.

Groß, F., Metzner, G., Behn, U., 2011. Mathematical modeling of allergy and specific immunotherapy:Th1–Th2–Treg interactions. J. Theor. Biol. 269, 70–78.

Hoare, R.L., Veys, P., Klein, N., Callard, R., Standing, J.F., 2017. Predicting CD4 T-cell reconstitution following pediatric hematopoietic stem cell transplantation. Clin. Pharmacol. Ther. 102, 349–357.

Höfer, T., Krichevsky, O., Altan-Bonnet, G., 2012. Competition for IL-2 between regulatory and effector T cells to chisel immune responses. Front. Immunol. 3, 268.

Jimenez, J.C., 2020. Bias reduction in the estimation of diffusion processes from discrete observations. IMA J. Math. Control Inf. 37, 1468–1505.

Jimenez, J.C., Yoshimoto, A., Miwakeichi, F., 2021. State and parameter estimation of stochastic physical systems from uncertain and indirect measurements. Eur. Phys. J. Plus 136, 1–17.

Karim, M., Bushell, A.R., Wood, K.J., 2002. Regulatory T cells in transplantation. Curr. Opin. Immunol. 14, 584–591.

Khailaie, S., Montaseri, G., Meyer-Hermann, M., 2020. An adaptive control scheme for interleukin-2 therapy. iScience 23, 101663.

Klein, M., Bopp, T., 2016. Cyclic AMP represents a crucial component of Treg cell-mediated immune regulation. Front. Immunol. 7, 315.

Köhler, N., Ruess, D.A., Kesselring, R., Zeiser, R., 2021. The role of immune checkpoint molecules for relapse after allogeneic hematopoietic cell transplantation. Front. Immunol. 12, 634435.

Liu, Z., Gerner, M.Y., Panhuys, N.V., Levine, A.G., Rudensky, A.Y., Germain, R.N., 2015. Immune homeostasis enforced by colocalized effector and regulatory T cells. Nature 528, 225–230.

Locke, F.L., Pidala, J., Storer, B., Martin, P.J., Pulsipher, M.A., Chauncey, T.R., Jacobsen, N., Kröger, N., Walker, I., Light, S., Shaw, B.E., Beato, F., Laport, G.G., Nademanee, A., Keating, A., Socie, G., Anasetti, C., 2017. CD25 blockade delays regulatory T cell reconstitution and does not prevent graft-versus-host disease after allogeneic hematopoietic cell transplantation. Biol. Blood Marrow Transplant. 23, 405–411.

Malek, T.R., Bayer, A.L., 2004. Tolerance, not immunity, crucially depends on IL-2. Nat. Rev. Immunol. 4, 665–674.

Matsuoka, K., Kim, H.T., McDonough, S., Bascug, G., Warshauer, B., Koreth, J., Cutler, C., Ho, V.T., Alyea, E.P., Antin, J.H., Soiffer, R.J., Ritz, J., 2010. Altered regulatory T cell homeostasis in patients with CD4+ lymphopenia following allogeneic hematopoietic stem cell transplantation. J. Clin. Invest. 120, 1479–1493.

Matsuoka, K., Koreth, J., Kim, H.T., Bascug, G., McDonough, S., Kawano, Y., Murase, K., Cutler, C., Ho, V.T., Alyea, E.P., Armand, P., Blazar, B.R., Antin, J.H., Soiffer, R.J., Ritz, J., 2013. Low-dose interleukin-2 therapy restores regulatory T cell homeostasis in patients with chronic graft-versus-host disease. Sci. Transl. Med. 5, 179ra43.

Matthews, K., Lim, Z., Afzali, B., Pearce, L., Abdallah, A., Kordasti, S., Pagliuca, A., Lombardi, G., Madrigal, J.A., Mufti, G.J., Barber, L.D., 2009. Imbalance of effector and regulatory CD4 T cells is associated with graft-versus-host disease after hematopoietic stem cell transplantation using a reduced intensity conditioning regimen and alemtuzumab. Haematologica 94, 956–966.

Merryman, R.W., Kim, H.T., Zinzani, P.L., Carlo-Stella, C., Ansell, S.M., Perales, M.A., Avigdor, A., Halwani, A.S., Houot, R., Marchand, T., Dhedin, N., Lescaut, W., Bertrand, A.T., Francqois, S., Bastard, A.S., Rohrlich, P.S., Wallet, H.L., Castagna, L., Santoro, A., Bachanova, V., Bresler, S.C., Srivastava, A., Kim, H., Pesek, E., Chammas, M., Reynolds, C., Ho, V.T., Antin, J.H., Ritz, J., Soiffer, R.J., Armand, P., 2017. Safety and efficacy of allogeneic hematopoietic stem cell transplant after PD-1 blockade in relapsed/refractory lymphoma. Blood 129, 1380–1388.

Miura, Y., Thoburn, C.J., Bright, E.C., Phelps, M.L., Shin, T., Matsui, E.C., Matsui, W.H., Arai, S., Fuchs, E.J., Vogelsang, G.B., Jones, R.J., Hess, A.D., 2004. Association of Foxp3 regulatory gene expression with graft-versus-host disease. Blood 104, 2187–2193.

Moatti, A., Debesset, A., Pilon, C., Beldi-Ferchiou, A., Leclerc, M., Redjoul, R., Charlotte, F., To, N.H., Bak, A., Belkacemi, Y., Salomon, B.L., Issa, F., Michonneau, D., Maury, S., Cohen, J.L., Thiolat, A., 2022. TNFR2 blockade of regulatory T cells unleashes an antitumor immune response after hematopoietic stem-cell transplantation. Journal for ImmunoTherapy of Cancer 10, e003508.

Nelson, B.H., 2004. IL-2, regulatory T cells, and tolerance. J. Immunol. 172, 3983–3988.

Nikiforow, S., Kim, H.T., Daley, H., Reynolds, C., Jones, K.T., Armand, P., Ho, V.T., Alyea, III, E.P., Cutler, C.S., Ritz, J., Antin, J.H., Soiffer, R.J., Koreth, J., 2016. A phase I study of CD25/regulatory T-cell-depleted donor lymphocyte infusion for relapse after allogeneic stem cell transplantation. Haematologica 101, 1251–1259.

Ozaki, T., 1994. The local linearization filter with application to nonlinear system identification. In: Bozdogan, H. (Ed.), Proceedings of the First US/Japan Conference on the Frontiers of Statistical Modeling: an Informational Approach. Kluwer Academic Publishers, pp. 217–240.

Pang, N., Duan, X., Jiang, M., Qu, J., Yuan, H., Xu, J., Cao, H., Chen, G., 2015. Reconstitution and clinical significance of T cell subsets in the early stage after related HLA-mismatched peripheral blood hematopoietic SCT without T-cell depletion in vitro. Int. J. Clin. Exp. Pathol. 8, 8892–8901.

Parmar, S., Ritchie, D.S., 2014. Allogeneic transplantation as anticancer immunotherapy. Curr. Opin. Immunol. 27, 38–45.

Perry, J.A., Clark, J.T., Gullicksrud, J., DeLong, J., Shallberg, L., Douglas, B., Hart, A., Konradt, C., Park, J., Glatman-Zaretzky, A., de Waal Malefyt, R., Christian, D.A., Sharpe, A.H., Hunter, C.A. PD-L1 – PD-1 interactions limit effector Treg cell populations at homeostasis and during infection. bioRxiv preprint. https://doi.org/10.1101/2020.12.09.416990

Roychoudhuri, R., Eil, R.L., Restifo, N.P., 2015. The interplay of effector and regulatory T cells in cancer. Curr. Opin. Immunol. 33, 101–111.

Sakaguchi, S., Yamaguchi, T., Nomura, T., Ono, M., 2008. Regulatory T cells and immune tolerance. Cell 133, 775–787.

Sansom, D.M., 2000. CD28, CTLA-4 and their ligands: who does what and to whom? Immunology 101, 169–177.

Setoguchi, R., Hori, S., Takahashi, T., Sakaguchi, S., 2005. Homeostatic maintenance of natural Foxp3+CD25+CD4+regulatory T cells by interleukin (IL)-2 and induction of autoimmune disease by IL-2 neutralization. J. Exp. Med. 201, 723–735.

Taylor, P.A., Noelle, R.J., Blazar, B.R., 2001. CD4(+)CD25(+) immune regulatory cells are required for induction of tolerance to alloantigen via costimulatory blockade. J. Exp. Med. 193, 1311–1318.

Toomer, K.H., Malek, T.R., 2017. Cytokine signaling in the development and homeostasis of regulatory T cells. Cold Spring Harbor Perspect. Biol.

Via, C.S., Finkelman, F.D., 1993. Critical role of interleukin-2 in the development of acute graft-versus-host disease. Int. Immunol. 5, 565–572.

Warwick, Kevin, 1996. An Introduction to Control Systems. second ed. World Scientific. ch. 10.3.

Winga, M.J.B., Osakia, M., Longa, J., Sakaguchi, S., 2021. Treg-expressed CTLA-4 depletes CD80/CD86 by trogocytosis, releasing free PD-L1 on antigen-presenting cells. Proc. Natl. Acad. Sci. U.S.A. 118, e2023739118.

Zhou, J., Bashey, A., Zhong, R., Corringham, S., Messer, K., Pu, M., Ma, W., Chut, T., Soiffer, R., Mitrovich, R.C., Lowy, I., Ball, E.D., 2011. CTLA-4 blockade following relapse of malignancy after allogeneic stem cell transplantation is associated with T cell activation but not with increased levels of T regulatory cells. Biol. Blood Marrow Transplant. 17, 682–692.

Zorn, E., Kim, H.T., Lee, S.J., Floyd, B.H., Litsa, D., Arumugarajah, S., Bellucci, R., Alyea, E.P., Antin, J.H., Soiffer, R.J., Ritz, J., 2005. Reduced frequency of FOXP3+CD4+CD25+ regulatory T cells in patients with chronic graft-versus-host disease. Blood 106, 2903–2911.